Research Square

Preprints are preliminary reports that have not undergone peer review.
They should not be considered conclusive, used to inform clinical practice,
or referenced by the media as validated information.

Humanity's Future Capacity for Physical Activity Limited by Climate Change and Population Aging

Haley Staudmyer

hstaudmy@uci.edu

University of California Irvine https://orcid.org/0009-0004-6806-9001

Jennifer K. Vanos

Arizona State University

Ollie Jay

University of Sydney https://orcid.org/0000-0002-6076-6337

Gisel Guzman Echavarria

Arizona State University

Qinqin Kong

School of Medicine, Stanford University https://orcid.org/0000-0002-4593-3643

Yudam Hwang

University of California Irvine

Sarah Perkins-Kirkpatrick

Australian National University https://orcid.org/0000-0001-9443-4915

Catherine H. Gregory

University of Bern

Jane Baldwin

University of California, Irvine https://orcid.org/0000-0002-4174-2743

Article

Keywords: climate change, extreme heat, health impacts, aging

Posted Date: August 12th, 2026

DOI: https://doi.org/10.21203/rs.3.rs-10593888/v1

License: This work is licensed under a Creative Commons Attribution 4.0 International License.
Read Full License

Additional Declarations: There is **NO** Competing Interest.

Humanity's Future Capacity for Physical Activity Limited by Climate Change and Population Aging

Haley Staudmyer[1*], Jennifer K. Vanos[2], Ollie Jay[3], Gisel Guzman-Echavarria[2], Qinqin Kong[4], Yudam Hwang[1], Sarah E. Perkins-Kirkpatrick[5,6], Catherine H. Gregory[7,8], Jane W. Baldwin[1]

[1*]Department of Earth System Science, University of California, Irvine, Croul Hall, Irvine, 92697-3100, CA, USA.
[2]School of Sustainability,Arizona State University, 777 E University Dr, Tempe, AZ 85281 , Tempe, 85281, Arizona, USA.
[3]Heat and Health Research Centre, University of Sydney, Western Ave, Camperdown, Sydney, 2006, NSW, Australia.
[4]School of Medicine, Stanford University, 450 Jane Stanford Way, Stanford, 94305, California, USA.
[5]Fenner School of Environment and Society, The Australian National University, 141 Linnaeus Way, Acton, Canberra, 2601, Australian Capital Territory, Australia.
[6]ARC Centre of Excellence for the Weather of the 21st Century, The Australian National University, 141 Linnaeus Way, Acton, Canberra, 2601, Australian Capital Territory, Australia.
[7]University of Bern, Hochschulstrasse 6, Bern, 3012, Switzerland.
[8]Oeschger Centre for Climate Change Research, University of Bern, Hochschulstrasse 4, Bern, 3012, Switzerland.

*Corresponding author(s). E-mail(s): hstaudmy@uci.edu;

Abstract

Sustained physical activity is necessary for society, but will become harder to safely accomplish. Using a physiology-based biophysical model of human heat stress risk with bias-corrected climate model projections and demographic models, we show that humanity's capacity for sustained physical activity while keeping core body temperature stable ("thermal compensability") decreases with

climate change and population aging over this century. At a 2°C global warming level, for adults in tropical regions, a physical activity intensity of household chores (3.3 METs) will be uncompensable 2.87% (2.25-3.98%) of the year; harvesting crops (4.8 METs) will be uncompensable for 37.69% (34.82-41.71%) of the year. Effects are worse for older adults and lessened at higher latitudes. Population aging drives significant global increases in heat risk; individual countries' primary heat risk drivers vary between climate and demographic changes. Our results underscore the urgent need for adaptation efforts that simultaneously address climate, physiology, and demographics.

Keywords: climate change, extreme heat, health impacts, aging

1 Introduction

Dry and humid extreme heat events are becoming more frequent, intense, and prolonged with climate change [1–4]. These changes affect both short-term heat waves and chronic heat stress [5]. Heat exposure poses a serious threat to human health; between 2011 and 2021, an average of 546,000 heat-related deaths occurred globally each year, with 37% of recent heat mortality attributable to climate change [6, 7]. Some studies project future heat-health impacts using exposure-response relationships estimated from historical population-level health data [8–10]; others project exceedances of critical thresholds of environmental heat stress metrics that combine temperature and humidity (e.g., wet bulb temperature, heat index) [11–15]. Alongside climate change, studies explore how demographic trends, especially the increasing proportion of older adults, may alter projected heat-health impacts. The global population will age throughout the 21st century, making people more vulnerable to heat, while increasing population density will expose more people to hot conditions [16–19]. Falchetta et al. found an additional 177–246 million older adults (69+) will be exposed to dangerous acute heat by mid-century [20].

Some physiology-informed heat-health projections examine "survivability" – how often conditions cause fatal heat stroke, assuming maximal behavioral adaptations, including resting nude in the shade [11, 21–24]. Recently, interest has grown in predicting heat-health outcomes beyond "survivability," given the wide range of essential activities societies require (e.g., working, caregiving, exercise) [25–29]. To explore the impacts of heat on safe physical activity, recent studies examine thresholds of human thermoregulatory "compensability" or "livability," i.e., where the body can physiologically compensate for exogenous and endogenous heat gain by triggering thermoeffector responses (e.g., sweating and cutaneous vasodilation) to maintain a stable core temperature [26, 28, 30]. "Uncompensable" heat stress conditions are not immediately fatal; however, prolonged exposure to uncompensable conditions without respite or decreasing metabolic load will eventually result in heat-stroke death [31, 32]. Compensability is modulated by a variety of factors [32, 72]. Beyond 65 years of age, ability to sweat declines, increasing heat vulnerability [27]. Global population aging therefore increases heat-health risks [8, 20].

How unsafe will everyday, necessary physical activity become over the next century given climate and demographic trends? Some studies examine projected heat limitations on heavy labor, others the prevalence of deadly conditions, but none explore a continuous range of activity levels and demographic diversity such as age [5, 21–24, 33, 34] simultaneously. Further, many commonly-used heat indices, models, and projections ignore human physiology or assume fixed physiology, and therefore cannot explore effects of aging or other physiological diversity [35]. Physiology-based human heat balance models can account for demographic and physiological diversity, but remain uncommonly used in projections due to their complexity and computational intensity. Consequently, we lack robust projections of human heat stress that integrate climate forcing with dynamic physiological limits that constrain human livability and labor potential.

To create more robust and applicable projections of heat stress risk, this study applies the recently developed ASU/USYD Human Environmental Adaptation and Threshold Limits (HEAT-Lim) model to an array of physiological profiles representing different age groups and bias-corrected climate change projections [26]. HEAT-Lim estimates the maximum level of activity (M_{max}), expressed in metabolic equivalents (METs), a human could sustain without entering an uncompensable state, using inputs of physiologic traits and environmental heat (temperature and humidity). Calculating how often M_{max} falls below a threshold provides insight into how restricted daily life could be. Previous work using HEAT-Lim showed that the range of livable activity has already decreased within the observed climate record for young and old adults [28]. Building on this, we assess how sustainable activity levels in the heat decrease with projected future global warming for people with differential thermoregulatory abilities. We examine how much of the year, on average, will be too hot for compensability at three key activity levels representative of harvesting crops, light household chores, and sitting, and calculate uncompensable "person-hours" representing population heat risk across age groups using future population density and age structure projections. We disentangle the relative impacts of climate change, population aging, and population density changes in driving future increases in heat risk at the country-level. We show that both climate change and demographic trends are important in limiting population-level physical activity over the next century. Climate change plays an increasingly important role as global warming intensifies.

2 Results

2.1 Global warm season physical activity limitations

Previous work applied HEAT-Lim to ERA5 data and found livability is most restricted in the tropics and other hot, humid regions [28]. Our results corroborate this: during the 1980-2010 historical period, warm-season average M_{max} for adults (age 20-64) was most restricted in the tropics, with Red Sea coasts of Saudi Arabia and Yemen reaching as low as 4.2 METs (comparable to brisk walking; Figure 1a). Globally, average warm-season M_{max} declines at a rate of -0.48 METs per degree of warming, from 7.34 METs during the historical baseline to 5.35 METs at 2°C warming (Figure 1c). On average, decreases are steeper in the subtropics (-0.53 METs/°C) and midlatitudes (-0.52

METs/°C) than in the tropics (−0.39 METs/°C) (Figure 1c). Polar regions and high-elevation regions face the smallest decreases in warm season average M_{max} (Figure 1b).

Warm-season adult M_{max} decreases are examined for twelve of the world's most densely populated cities (population >15 million; Methods, 4.5.1). In 7 of 12 cities, average warm season M_{max} decreases more steeply than the corresponding latitude-band average (Figure 1d), likely reflecting local factors like elevation or coastal proximity and associated humidity. Cities in continental interiors (e.g., Moscow) or at higher elevation (e.g., São Paulo) show smaller declines than their band average. In the two most heat-stressed cities in the historical baseline, warm-season M_{max} falls below 3.3 METs at 4°C GWL (less than the M_{max} required for household chores).

Corresponding Figure 1 versions for three other age profiles—children (aged 10–19), old adults (65–84), and very old adults (85+)—under both SSP5-8.5 and the more moderate SSP2-4.5 scenario are available in the Supplemental Material (Figures S1-S2; Supplementary Results). Children maintain higher absolute M_{max} than adults across most GWLs due to near-ceiling baseline values, but experience faster M_{max} declines in hot, tropical environments; old and very old adults decline at rates similar to, but smaller than, adults (Supplementary Results).

2.2 Time per year under key physical activity thresholds

We examine how often M_{max} falls below three key activity thresholds. Less extreme heat and/or humidity is required for M_{max} to reach 4.8 METs (comparable to harvesting crops with moderate effort; Figures 2a, c, e) than for 3.3 METs (comparable to doing household chores; Figures 2b, d, f), so the 4.8 METs threshold is reached more regularly worldwide. The greatest increases in time spent with $M_{max} < 3.3$ METs occur in places already activity-limited in the baseline period: the Indo-Gangetic Plain, the United Arab Emirates, and Qatar go from ∼5%–6% of the year below this threshold at baseline to ∼13%–15% of the year at 2°C, indicating that activity is severely limited by heat stress for a substantial portion of the year. Other locations, like the midlatitudes, rarely experience this limitation up to 2°C warming.

Regions with the greatest percentage of year with $M_{max} < 3.3$ METs are no longer hotspots under a $M_{max} < 4.8$ METs threshold, since a substantial portion of the average historical year is already spent under this less-restrictive threshold in the tropics (e.g., ∼22% of the year in the tropics, Figure 2d); instead, the greatest increases occur in other hot, humid, tropical areas, such as the Amazon, Oceania, southeast Asia, and west Africa. The tropics exhibit the steepest increases in both threshold-based metrics, sitting naturally closest to the thresholds in the historical period – a pattern seen across other threshold-based heat metrics [36]. Coastal areas or areas proximal to water features (e.g., the Amazon River) show larger increases, likely due to locally-elevated humidity.

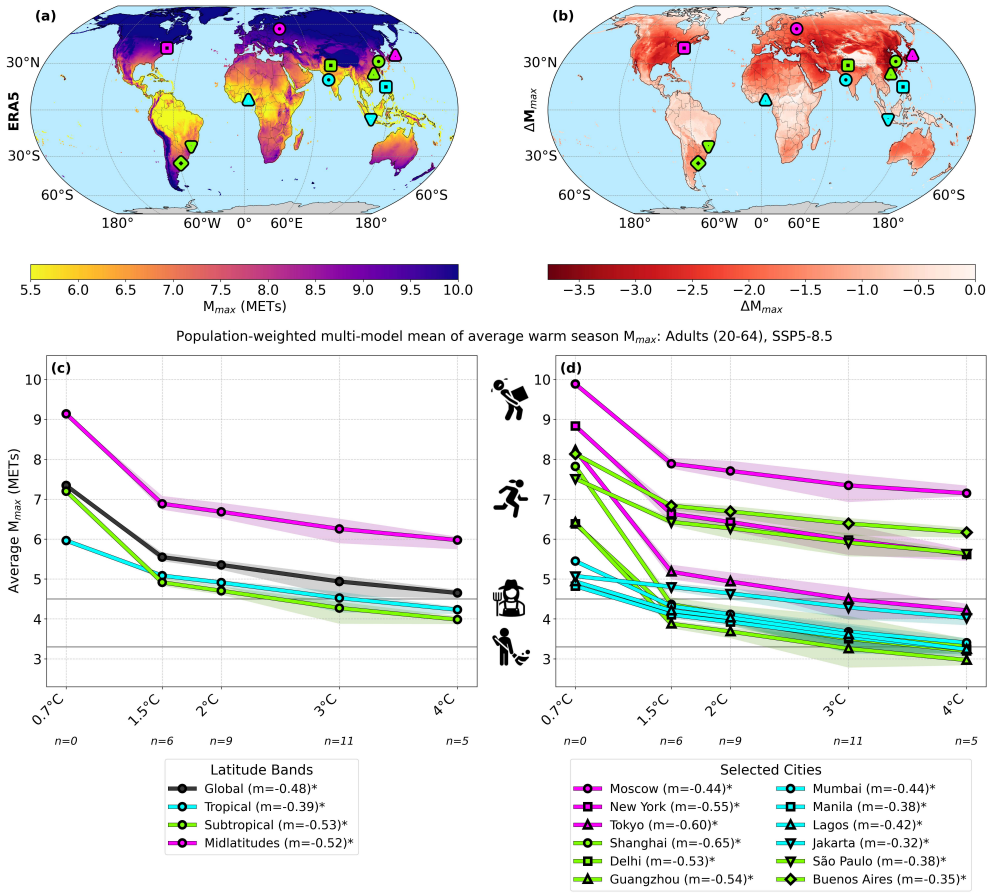


Fig. 1 Average warm season M_{max} decreases with global warming level (GWL) for adults (age 20-64). "Warm season" is defined separately in each grid cell as the hottest day of the year, determined using the ERA5 climatology (1980-2010), and the 91-day period surrounding that day. **a)** Spatial pattern of warm season M_{max} averaged over the ERA5 climatology. Twelve populous cities (population >15 million; Methods 4.5.1) are marked, colored by latitude band (tropics, cyan; subtropics, green; midlatitudes, magenta; Methods 4.3 for exact ranges). **b)** Bias-corrected, multi-model average spatial pattern of warm season M_{max} during a 20-year 2°C GWL period, shown as the difference from the ERA5 climatology in (a). **c)** Warm season M_{max} at each GWL, averaged over global land grid cells (black) or population-weighted latitude bands (colored as in (a) and (b)). 0.7°C represents the ERA5 climatology baseline period (Methods 4.3). Shaded area represents the multi-model range. Slopes from scatter regressions across all individual model data points are noted in legend (m, METs/°C); asterisks denote statistical significance ($p < 0.05$). Labels underneath the x-axis (n =) denote the number of climate models available at each GWL. Horizontal gray lines denote M_{max} thresholds of interest, 3.3 and 4.8 METs. The light gray, hatched region between 3°C and 4°C denotes fewer available climate models, as not all models reach 4°C. **d)** As in c, but for individual grid cells centered on the twelve populous cities. Icons between panels (c) and (d) represent the approximate activity level denoted by the corresponding M_{max} values on the y-axes.

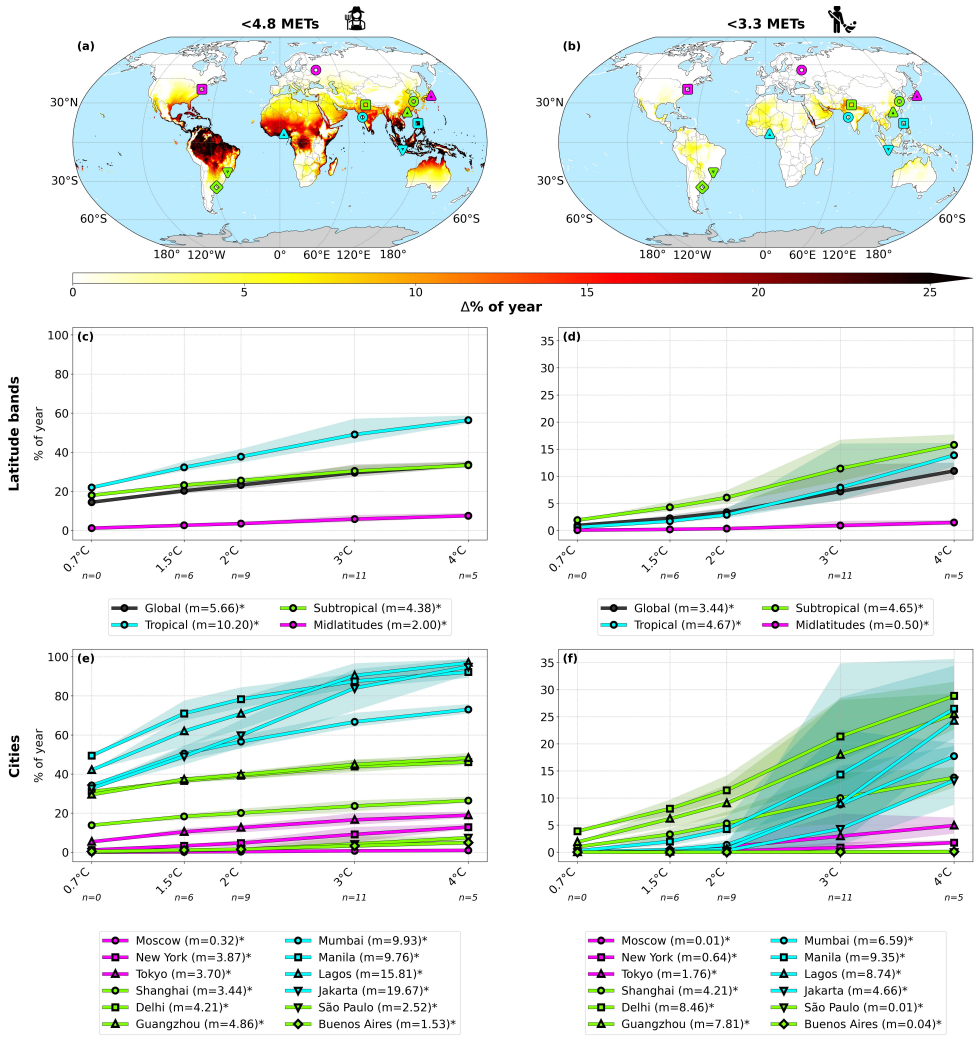


Fig. 2 Change in amount of time per year spent under key M_{max} thresholds for adults (age 20-64). a) Bias-corrected, multi-model average percentage increase at a 2°C GWL relative to the baseline period (1980-2010) in time per year where $M_{max} < 4.8$ METs, a level of physical activity comparable to that needed to harvest crops and accomplish farmwork with moderate effort. As in Figure 1, 12 populous cities are marked, colored by latitude band (tropics, cyan; subtropics, green; midlatitudes, magenta; Methods 4.3 for exact ranges). **b)** As in a, but for $M_{max} < 3.3$ METs, a level of activity comparable to that needed to do light household chores. **c)** Change per degree of global average warming in multi-model average time spent where $M_{max} < 4.8$ METs, as a percentage of an entire year (Methods 4.3), averaged over land pixels of the entire globe (black) or latitude bands (colored analogously to the city markers in a and b). Shaded area surrounding lines represents the multi-model range. Slopes from linear regressions (dashed lines), calculated using data through the 4°C GWL, are noted in legend (m, % of year per °C). Labels underneath the x-axis ($n =$) denote how many climate models had data available at the associated GWL. The light gray, hatched region between 3°C and 4°C denotes fewer available climate models, as not all models reach 4°C. **d)** As in c, but for a threshold of $M_{max} < 3.3$ METs. **e)** As in c, but for the twelve populous cities. **f)** As in e, but for a threshold of $M_{max} < 3.3$ METs.

With warming, available time per year, on average, for compensable activity will decrease across both thresholds considered (Figures 2c-f). In the global average at a 4°C GWL, just over 10% of the year is spent with $M_{max} < 3.3$ METs (Figure 2C). However, Delhi exceeds that milestone at a 2°C GWL, with $M_{max} < 3.3$ METs for 11.5% of the year, compared 3.9% in the baseline period.

Given that less extreme conditions are needed to pass the $M_{max} < 4.8$ METs threshold, greater portions of the average year will be spent under it. The greatest changes will be seen in the tropics, where, for every degree of global average warming, an additional 10.2% of a year sees conditions where moderate activity is uncompensable. Across all tropical cities examined, 56-78% of the year, on average, falls under this threshold at a 2°C GWL, compared to 32-49% in the baseline period. However, the rate of change per degree is lower for certain cities at this threshold than the $M_{max} < 3.3$ threshold (i.e., Shanghai, Delhi, and Guangzhou). Given that a larger portion of their average year already existed under the $M_{max} < 4.8$ threshold in the historical record, increases are more limited to shoulder seasons. Uncertainty across models is large for some estimates with the more extreme < 3.3 METs activity threshold, especially growing at the 3°C GWL to span 5.6-16.0% of the year for the tropics on average, and 1.6-35% and 9.2-28.6% for Lagos and Manila, respectively.

This analysis was repeated for the three additional age groups and under the more moderate SSP2-4.5 scenario (Figures S3-S5; Supplementary Results); despite differences in climate model availability, patterns are qualitatively similar between scenarios. As with adults, uncompensable time per year increases with GWL across all age groups and thresholds, always most severely in the tropics (Figure 3). Children fare better than adults, whereas old and very old adults fare worse: under the $M_{max} < 4.8$ METs threshold at 2°C GWL in the tropics, this reaches 13%, 38%, 59%, and 73% of the year for children, adults, old adults, and very old adults, respectively. Elderly age groups face substantial heat risk even outside the tropics: at 2°C GWL, old and very old adults spend 34.96% and 43.08% of the year, respectively, under the $M_{max} < 4.8$ METs threshold in the midlatitudes/subtropics (Supplementary Results).

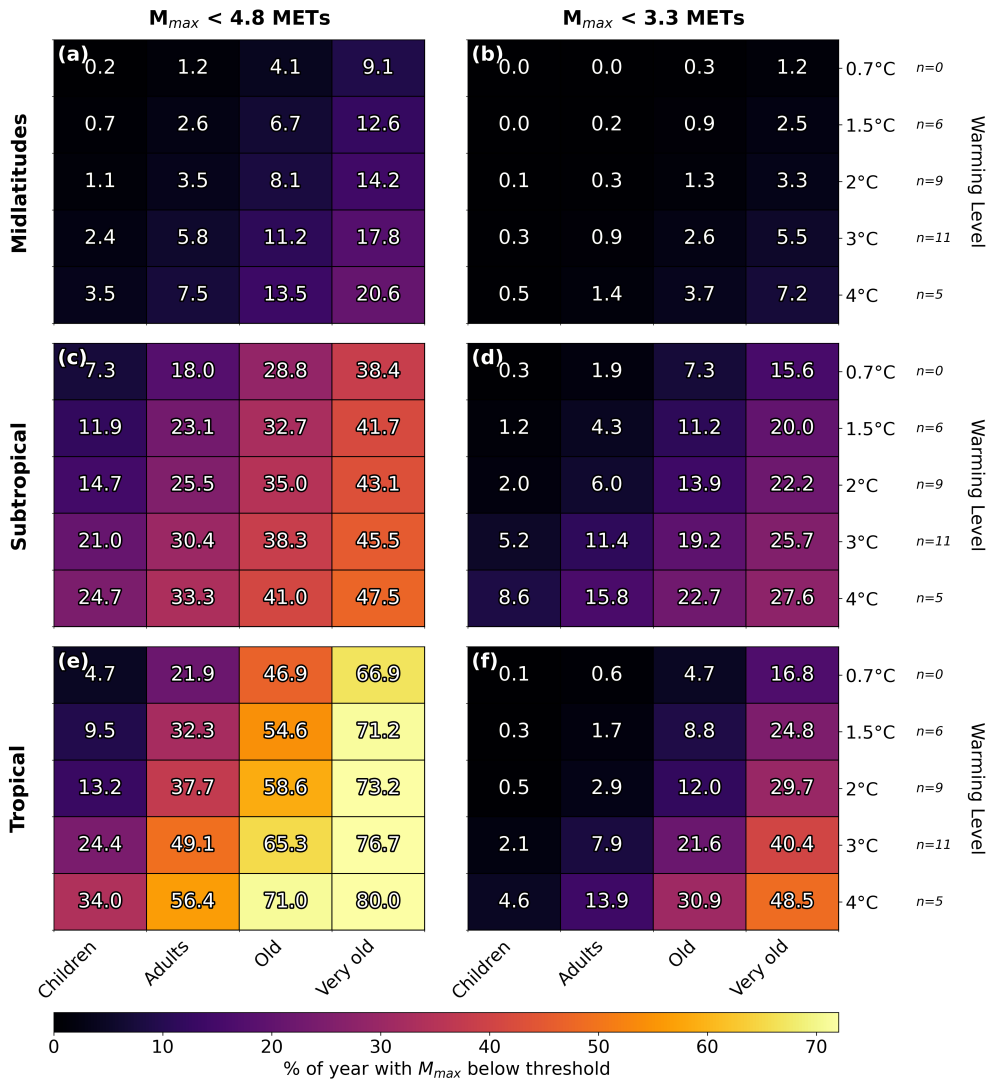


Fig. 3 Amount of time per year spent under key M_{max} thresholds for different age groups and GWLs. Multi-model average time spent where $M_{max} < 4.8$ METs (a-c) or $M_{max} < 3.3$ METs (d-f), measured as a percentage of an entire year, for four different age groups (children (10-19), adults (20-64), old adults (65-84), and very old adults (85+)), five different GWLs (0.7°C, representative of the 1980-2010 ERA5 climatology period, as well as 1.5°C, 2°C, 3°C, and 4°C), and three different latitude bands. Labels by the y-axis ($n =$) denote how many climate models had data available at the associated GWL.

In addition to the 4.8 and 3.3 MET thresholds, we identify where and at what warming level conditions that are survivable but not truly "livable," i.e., where even minimal physical activity is uncompensable, first emerge in the model ensemble. Such conditions are rare for children and adults in the historical climate, but expand across parts of the tropics for adults by 1.5°C GWL and to nearly half of all land area for the oldest adults by 3–4°C GWL, eventually reaching even high-latitude regions (Supplementary Figure S6, Supplementary Results); the same pattern holds under the more moderate SSP2-4.5 scenario (Supplementary Figure S7, Supplementary Results).

2.3 Country-level drivers of future physical activity limitations

To examine the relative impacts and interactions among three separate drivers of future population risk of livability-limited conditions – climate change, aging, and population density – we estimate total person-hours per year (PH/yr), summed globally across all land grid cells, experienced under key M_{max} thresholds at different GWLs. Person-hours – calculated as the number of hours per year a threshold is breached, multiplied by the number of people in a location and the proportion of that population in a given age group (Methods, 4.6) – capture both the duration and demographic scale of heat exposure in a single metric, enabling direct comparison of risk magnitude across countries, age groups, and time. We explore which drivers contribute the most to future increases in PH/yr across countries (Figure 4; Methods, 4.6). Results are reported using SSP5-8.5 alignment of population and climate projections (Methods 4.5.2); corresponding SSP2-4.5 results are qualitatively similar, though demographic drivers contribute somewhat more under this scenario (Methods 4.5.2 and Figure S8, Supplementary Results).

PH/yr increases sharply with warming for both thresholds (Table 1; Figure 4a,c). We additionally report PH/yr in workdays per year (workdays/yr), where one workday equals 8 person-hours. These totals are larger under the more moderate SSP2-4.5 scenario at a given GWL, since each warming level is reached later in time, when the population is larger and older (Table S1, Supplementary Results).

Table 1 Total person-hours per year (PH/yr) and workday-equivalents (workdays/yr), both in billions, under key M_{max} thresholds and global warming levels (GWL), for SSP5-8.5. Percent change is relative to the 1980-2010 ERA5 historical baseline (0.7°C GWL). The SSP2-4.5 equivalent of this table is provided as Table S1, Supplementary Results.

	M_{max} < 3.3 METs			M_{max} < 4.8 METs		
GWL	PH/yr	Workdays/yr	% chg	PH/yr	Workdays/yr	% chg
Baseline (0.7°C)	13.9	1.74	–	195	24.4	–
1.5°C (avg. 2032)	61.0	7.63	+337%	439	54.9	+125%
2°C (avg. 2042)	102	12.7	+629%	555	69.4	+184%
3°C (avg. 2060)	220	27.4	+1474%	764	95.6	+291%
4°C (avg. 2070)	315	39.4	+2158%	885	110.7	+353%

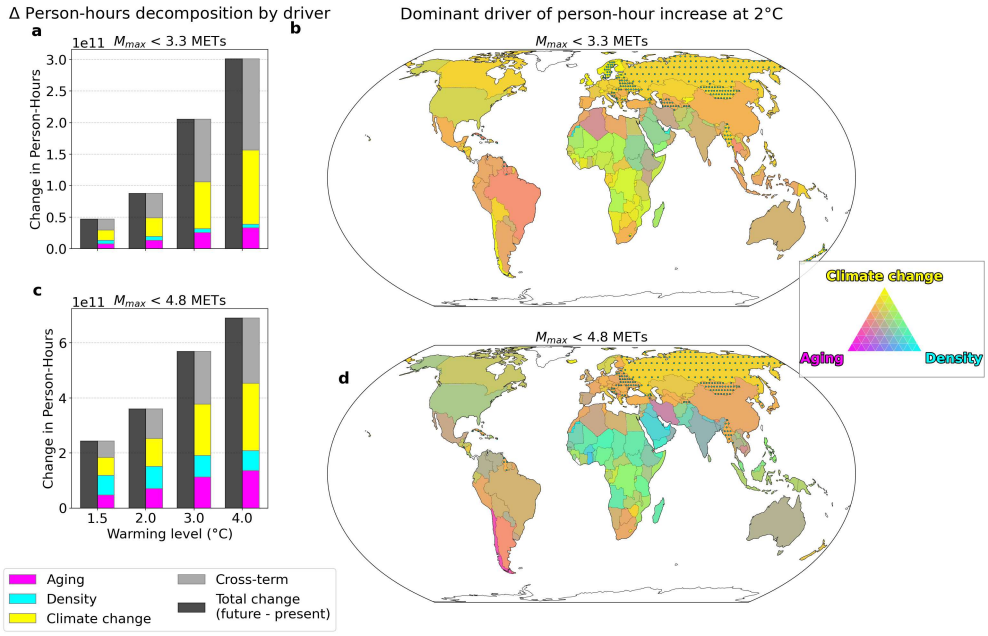


Fig. 4 Drivers of global person-hours below key M_{max} thresholds. a) Total global change in person-hours per year (PH/yr), summed across all land grid cells, at risk of conditions with $M_{max} < 3.3$ METs (an activity level representative of light household chores). Total change is calculated as the difference in PH/yr between the 1980-2010 ERA5 climatology period and each GWL of interest (dark gray). Changes in PH/yr in scenarios where only a single driver (aging, density, or climate change) is allowed to evolve from the ERA5 climatology period (Methods, 4.6) are denoted by the thinner, colored stacked bars, with aging in magenta, population density in cyan, and climate change in yellow. The difference between the sum of the stacked bars and the total change (dark gray) is the cross-term (representative of the interactions among drivers), shown in light gray. **b)** Countries of the world shaded by which drivers (aging, in magenta, population density, in cyan, and/or climate change, in yellow) contribute the most to that country's increased future (2°C GWL) PH/yr where $M_{max} < 3.3$ METs. Colored stippling indicates that one of the three drivers made a negative contribution to future person-hours; which of the three drivers is denoted by the color of the stippling (Methods, 4.6). If one of the three drivers provides a negative contribution to future PH/yr in a country, that driver does not contribute to the country's color of shading. Countries for which fewer than 50% of the country's population falls within the shared valid-data domain across all three driver datasets (Methods, 4.6) are left unshaded, as their classification would otherwise rest on an unrepresentative fraction of the country's population; this affects Greenland and a small number of small island nations, none of which are discussed individually in the text. **c) d)** As in (a) and (b), but using a threshold of $M_{max} < 4.8$ METs (an activity level representative of harvesting crops) to calculate PH/yr.

Using the $M_{max} < 3.3$ METs threshold to define hot-hours, we find that globally, increases in future PH/yr are driven primarily by population aging and climate change, with population density increases playing a smaller role (Figure 4a). Climate change has a larger effect than aging at 1.5°C and 2°C GWL, though aging remains a substantial secondary driver (i.e., at 1.5°C and 2°C GWL, the effect of aging is 48.3% and 45.1% of the effect size of climate change, respectively). At higher GWLs, the

effects of climate change worsen and outpace the effects of aging (i.e., at 4°C GWL, the effect of aging is 28.3% the size of the effect of climate change). The cross-term, representing the interactions among drivers, increases over time. More people – particularly, older people – experiencing a hotter climate leads to compounding impacts among drivers and a positive cross-term.

Changes in population density become more important using a threshold of $M_{max} < 4.8$ METs to define hot-hours, since people of all age groups experience this less-strict threshold more often (Figure 3); for example, 22.2% of the increase in PH/yr with $M_{max} < 4.8$ METs is due to population density at a 2°C GWL, versus just 7.25% for $M_{max} < 3.3$ METs. Otherwise, the general pattern of individual driver contributions in Figure 4c (3.3 METs) remains similar to those seen in Figure 4a (4.8 METs) – demographic (aging and density) effects have contributions similar or greater in size to those from climate change at smaller GWLs (e.g., 59.8% from both demographic drivers at 2°C GWL, compared to 40.2% from climate change), but at higher GWLs, effects from climate change outpace those of demographic changes (e.g., 45.8% from both demographic drivers combined at 4°C GWL, compared to 54.2% from climate change alone). At higher GWLs, the effects of population density as a driver of PH/yr stall out as the global rate of population density increase slows down. The cross-term increases in size with GWL, and is consistently larger than for the $M_{max} < 3.3$ METs threshold.

The main driver of future PH/yr increase varies widely by country and depends on the chosen M_{max} threshold (Figures 4b and 4d). Developed, wealthier, extratropical countries are more likely to have future increases dominated by aging population and/or worsening effects of climate change. Higher-latitude countries tend to have increased effects from climate change due to the rarity of reaching these thresholds in the historical climate at these high latitudes paired with Arctic amplification of warming. In contrast, low- and middle-income countries (LMICs) experience a proportionally larger impact from population density increases. LMICs' populations are rapidly growing, and although most of them are aging, their historical median age is very low; an aging population thus does not necessarily push an equivalently large portion of the population into the >65 age bracket. This effect is more pronounced under a $M_{max} < 4.8$ METs threshold (Figure 4d), since this threshold more readily affects people of all ages (Figure 3).

In some tropical and subtropical countries, the time spent under the $M_{max} < 4.8$ METs threshold during the baseline was already a significant portion of the year (Figures 2a, c, e). Since there is less opportunity to increase the number of hot-hours per year – particularly for the 4.8 METs threshold – less of the increase in person-hours is driven by climate change as compared to more poleward countries. Climate change plays a larger role for the more stringent $M_{max} < 3.3$ METs threshold because $M_{max} < 3.3$ METs conditions do not occur in most places in the historical climate, but become more widespread with warming. This effect is particularly clear in some densely-populated tropical cities (i.e., see Jakarta, Figure 2f).

3 Discussion

This analysis quantifies the impacts of extreme heat on human health using a novel physiology-based biophysical model of human heat stress risk. Our work moves beyond metrics of "survivability" to quantify "livability," allowing decreases in physical activity capacity to be quantified without choosing a particular activity threshold (Results, 2.1). Furthermore, we demonstrate that even light levels of activity, such as completing household chores, will become uncompensable for longer periods of the average year (Results, 2.2). Previous work showed that humanity's capacity for compensable activity and labor has decreased throughout the observed satellite record [27, 33, 37]. Projecting to the future, Dunne et al (2013) found that population-weighted individual labor capacity would be reduced to 80% of its potential in peak months of heat stress by 2050; Nelson et al (2024) found physical work capacity will be reduced to 70% of full work capacity by end-of-century SSP5-8.5 conditions [33, 37]. While these results cannot be directly compared to ours given methodological differences (e.g., assumed activity level, shading assumptions), our results similarly show that safe time for physical activities necessary for daily life and societal function will shrink globally (e.g., only 77% and 66% of the year will be compensable for adults performing activity of 4.8 METs at a 2°C and 4°C GWL, respectively, compared to 86% in the historical climate). The steepest increases in uncompensable time are seen in the tropics and subtropics, a spatial pattern corroborated by prior work [34, 38, 39].

Crucially, diminished capacity for physical activity is not driven by climate change alone. Heat is known to be deadly for the elderly, as older bodies are less able to compensate for heat due to age-related decrements in sweating [27]. Previous epidemiology-based work found between 20%—25% of heat deaths will be attributable to population aging between 1.5-3°C GWL [8]. Our results show a comparably-sized effect: at the 4.8-MET threshold, aging accounts for approximately 19-20% of the total increase in PH/yr across this same GWL range (Figure 4c). Aging plays a larger role at the higher M_{max} threshold because, in milder conditions, younger age groups can still compensate for heat by sweating; in more extreme conditions at the 3.3-MET threshold, M_{max} for all age groups converges toward the model's physiological floor, an effect also visible in some hot areas at the historical baseline (Supplementary Figure S6, Supplementary Results). Children's disproportionate vulnerability specifically in hot, tropical conditions (Results 2.1) likely reflects a distinct physiological mechanism tied to body size rather than sweating capacity. Our children profile differs from the adult profile only in height and weight (Methods 4.1), children's smaller body size increases their surface area:mass ratio, and HEAT-Lim's dry heat exchange terms scale with body surface area [26]. This ratio favors heat dissipation when ambient and radiant temperatures remain below the model's assumed skin temperature, as is typically the case in the midlatitudes, but becomes a liability once these temperatures exceed skin temperature, as increasingly occurs in the tropics.

Primary drivers of increasing population heat risk vary by country, GWL, and M_{max} threshold defining hot-hours. At lower GWLs (e.g., 1.5°C—2°C), the impacts of climate change and demographic shifts contribute similarly to the overall risk increases. However, at higher GWLs, more frequent activity-limiting heat induced by climate change outpaces demographic trends as the dominant driver of increased risk. For

lighter activities (3.3 METs), climate change has a larger effect on person-hours than demographic drivers because conditions severe enough to restrict such light exertion are rare in the baseline climate. The effects of population density are stronger at the moderate activity threshold (4.8 METs), as this less-extreme physiological limit more commonly affects larger swaths of the population at all ages.

Geographic disparity in drivers highlights distinct, localized vulnerabilities. In developed, high-income nations experiencing stagnating or declining population growth, future risk is driven almost entirely along the climate-aging axis. Conversely, in fast-growing LMICs – particularly in Africa – population density increases drive future risk of heat stress. The cross-term interactions between climate change, aging, and population density are positive; a hotter climate compounds with the vulnerability of an older, denser population, and this compounding grows with GWL. This pattern is corroborated by independent, observation-based evidence: analyzing global heat stress via the Universal Thermal Climate Index, Emerton et al (2026) similarly found that recent rise in population heat exposure is driven by climate change and population growth, with climate change contributing at least as much as population density growth for most exposure categories [4].

Several limitations contextualize these projections. The reduction of the global population into four discrete physiological profiles is a necessary simplification given HEAT-Lim's current capacities; however, it does not capture all physiological modulators of thermoregulatory capacity, such as pregnancy or underlying medical conditions. To remain conservative in our estimates of age-related impacts, we assumed young-adult-like thermoregulatory capacity is maintained up to age 65 for our adult (20-64) profile. Age-related decrements in sweating are well-documented at 65+ years, but some studies observe reductions in sweat output as early as 45-50 years [40]. Our adult profile's results should therefore be interpreted as a conservative estimate of heat risk. Furthermore, M_{max} calculated by HEAT-Lim reflects the activity level thermally compensable under prevailing heat stress; it does not incorporate age-related declines in aerobic capacity (VO_2max) or the cardiovascular strain of heat exposure (e.g., competing skin and muscle blood flow demands), both of which independently constrain sustained activity and may fall below HEAT-Lim's thermal ceiling for the oldest adults, particularly at the higher M_{max} values considered here [41].

Future work should explore the sensitivity of HEAT-Lim to the various assumptions made here. HEAT-Lim is validated exclusively for heat stress; exploring M_{max} increases during the cold season is outside the scope of this work. The climate projection bias-correction methodology we use accounts for thermodynamic changes in seasonal climate but negates dynamic changes in weather variability with warming, suggested to affect future frequency of heat waves [42]. HEAT-Lim was applied assuming full shade and a wind speed of 1 m/s, but in reality, radiation and wind speed may be affected by climate change [43, 44]. Future population age structure projections used here are limited to country-level resolution [45]. Many countries would benefit from in-depth, individual analysis that was beyond the scope of this work.

Reductions in human ability to accomplish necessary physical activities in compensable conditions negatively affect human agency and economic independence. The expansion of conditions with limited possible activity and emergence of "survivable

but not livable" conditions across age groups means that vast swaths of the global population – particularly the elderly and those in humid, tropical LMICs – will increasingly be unable to safely work, care for themselves, and maintain their daily lives. We emphasize that these projections describe a loss of comfortable functional capacity, not necessarily mortality risk – but even where uncompensable heat stress is not immediately fatal, the widespread erosion of capacity for basic daily activity represents a substantial and growing threat to human wellbeing and quality of life. Limiting global average warming to 2°C by mitigating greenhouse gas emissions would greatly reduce the amount of human risk to livability-limited conditions. Limiting warming further to 1.5°C would present noticeable, but more manageable, changes to humanity's capacity for activity than 2°C of warming. However, climate mitigation alone will not be sufficient to protect all populations from worsening heat risk: in a small number of countries – including Chile, Kosovo, and Iran – population aging is projected to be the single largest driver of increased heat risk by a 2°C GWL, exceeding the direct contribution of climate change itself, underscoring the need for targeted protection of aging populations. In any outcome, substantial heat adaptations will be necessary to ensure human wellbeing, including but not limited to working earlier or later in the day when conditions are cooler, targeted heat warning systems for vulnerable populations, cooling centers, and expanding green space; these efforts should prioritize solutions that do not themselves exacerbate climate change (i.e., carbon-intensive air conditioning) [39, 46].

4 Methods

4.1 HEAT-Lim model, configuration, and application

The ASU/USYD Human/Environmental Adaptation and Threshold Limits Model (HEAT-Lim) is a physiology-based biophysical model estimating risk of human heat stress and strain [26]. It estimates whether a human body can adequately compensate for the prevailing environmental conditions and maintain safe core body temperatures. Environmental conditions considered include ambient temperature, humidity, surface pressure, air velocity, and mean radiant temperature. If these environmental conditions are "livable" – i.e., at least a small amount of physical activity (1.5 METs or more) is compensable – HEAT-Lim then calculates the maximum metabolic heat production, translated into intensity of physical activity, that is permissible while remaining compensable (i.e., no sustained increases in core body temperature). Physical activity is reported in metabolic equivalents, or METs. A higher maximum level of compensable METs (M_{max}) indicates lower environmental heat stress (environment allows for more intense safe physical activity). HEAT-Lim estimates different M_{max} values for different body morphologies and ages by adjusting constants associated with the human body's physiological characteristics (e.g., body size, sweat capacity). While HEAT-Lim can also be used to assess survivability – whether a human could avoid heat stroke and death when conditions are not livable (complete rest) – the current study assesses "livability" only (Case 2 in Figure 1 of Parsons et al 2026 [28]), i.e., where some amount of physical activity typical of everyday life is compensable. The model

is fully described in the supplemental material of Vanos et al (2023). The latest version of the model code is available in a Zenodo repository [47]; the code used in the climate model applications in the current study is available on GitHub [48].

Here, we define four different sets of physiological constants – height, mass, body surface area, sweat rate, and maximum skin wettedness – broadly representative of four age groups ("profiles") (Supplementary Information Table S3): children (aged 10–19), adults (20–64), old adults (65–84), and very old adults (85+). Supported by recent studies, the 10–19-year-old age group differs from the 20–64-year-old age group only in body size (height, mass, and body surface area); sweat rate and maximum skin wettedness are shared between the two groups [49–51]. Less is known about the sweating capabilities of children aged 0–10 due to a lack of empirical studies and related safety concerns; hence, this age group was not considered in the present analysis. For "old" and "very old" adults, sweating capabilities are physiologically reduced [52–54], and population-average body mass is modestly lower than for the broader 20–64 adult bracket, consistent with reported declines in body mass in the oldest age groups following a peak in mid-adulthood [55–57]. All profiles are assumed to be partially heat acclimatized. See the Supplementary Material for a full description of the HEAT-Lim constants for each age group, and the related justification. Note that the profiles considered are approximations of an average person in each group – in reality, the physiological constants in question also vary among individuals within age groups. While we acknowledge that the profiles simplify the world's population to only four subgroups of physiologic traits, our approach is a substantive step beyond existing heat stress projections, which do not account for physiological differences in heat stress thresholds across demographic groups based on thermoregulatory ability, nor consider children. Future work may explore a broader range of these physiological characteristics.

We assume a constant wind speed of 1 m/s due to the unreliable nature of surface wind speed projections within the boundary layer at high temporal resolution in climate models [58]. Parsons et al (2026) examine the sensitivity of HEAT-Lim M_{max} to wind speed and find that its effect on livability is non-monotonic: higher wind speeds generally improve livability in humid heat by increasing convective and evaporative cooling, but degrade it in hot, dry extremes where air temperature exceeds skin temperature; a mid-range baseline assumption of 1 m/s therefore avoids overstating either effect [28]. Likewise, rather than testing multiple sun/shade conditions, we test only a fully-shaded condition to provide a conservative estimate of heat risk. Testing sensitivity to these choices was beyond the computational feasibility for this analysis. We choose to direct finite computational resources into testing different personal profiles. Given that HEAT-Lim was designed for heat exposures and does not represent thermoeffectors for cold stress, any M_{max} values calculated above 10 METs are considered unreliable and therefore capped to 10 METs.

In the results, latitude bands are defined as 23° S–23° N for the tropics, 23° N/S–35° N/S for the subtropics, and 35° N/S–60° N/S for the mid-latitudes. The 60° N/S–90° N/S polar latitude band is excluded from analyses given that most land areas never reach livability-limited conditions. In Figure 2c-f and Figure 3, where percentages

of a year under a particular M_{max} threshold are reported, 365 days (8,760 hours) in an average year is equal to 100%.

4.2 Climate datasets

Climate model output at sub-daily temporal resolution is preferable for analyzing heat risk to capture the diurnal cycle and include peak heat hours. Thus, we limited our analysis to 12 Coupled Model Intercomparison Project – Phase 6 (CMIP6) climate models that provide 3-hourly data for 2-m temperature (T), 2-m specific humidity (q), and surface pressure (p) following either or both of the SSP5-8.5 and SSP2-4.5 scenarios (Supplementary Table S2) [59]. Unless otherwise noted, all main-text figures and results use SSP5-8.5 (a high-emissions scenario reflecting continued fossil-fuel-intensive development); corresponding results under the more moderate SSP2-4.5 scenario are provided in the Supplementary Information. Our analysis is oriented around global warming levels (GWLs) rather than calendar time: GWL periods are calculated independently for each model and scenario (Methods 4.3), so they may differ across climate models even at the same GWL. Only the "r1i1p1f1" ensemble member of each climate model was used, except for FGOALS-g3 under SSP2-4.5 scenario, where "r1i1p1f1" output was not available and"r3i1p1f1" output was used instead. To calculate warming levels relative to the preindustrial period, we also used CMIP6 2-m temperature output during 1850–1900 (Methods 4.3), though this was taken on a daily temporal resolution for certain models that did not have 3-hourly temperature for the preindustrial period (Supplementary Table S2).

We also use outputs from the European Centre for Medium-Range Weather Forecasts Reanalysis version 5 (ERA5) [60] to provide an observation-based historical baseline against which to compare and bias correct CMIP6 projections. Specifically, we use hourly 2-m air temperature, 2-m dewpoint temperature, and surface pressure estimates over land, which we average to 3-hourly temporal resolution for comparison with climate model output. See below (Methods 4.4) for the bias-correction methodology.

4.3 Warming level calculations

Comparing climate models at specified GWLs, rather than at a fixed calendar year, controls for inter-model differences in climate sensitivity (the amount of warming a model produces for a given level of radiative forcing), and provides impact assessments relevant to global climate action agreements (e.g., the Paris accords) [61, 62]. For this analysis, we calculated time periods representative of 1.5°C, 2°C, 3°C, and 4°C of global average warming relative to a 1850–1900 baseline in each model projection following methodology outlined by Seneviratne & Hauser (2020) [63]. The number of models contributing to the multi-model mean at each GWL varies by scenario and is not monotonic with warming level (Supplementary Table S2); it is smallest at the highest GWL reached within each scenario – 5 of 12 models reach 4°C under SSP5-8.5, and 5 of 12 reach 3°C under SSP2-4.5, which does not reach 4°C at all within the models considered here. Thus, analysis at 4°C GWL is impossible under SSP2-4.5, and results at the highest GWL reached under each scenario are less representative of inter-model variability than at lower or intermediate GWLs.

To compare with the ERA5 climatology (1980–2010), it is necessary to calculate the GWL of this period. We use the HadCRUT5 observational dataset to calculate a GWL of 0.7°C for the 1980–2010 climatology period as compared to the 1850–1900 baseline [64].

4.4 Bias-correction

CMIP6 model output is bias-corrected using ERA5 reanalysis following the same methodology outlined in Kong & Huber (2025) with minor modifications [59, 60, 65]. Broadly, this process derives the climate change signal at a given GWL from each climate model and then applies the signal to an ERA5 baseline. ERA5 near-surface temperature (T) and pressure (p) were obtained at a 3-hourly temporal interval, as well as near-surface dewpoint temperature, which was then converted to specific humidity (q) using the MetPy Python package in preparation for use in bias-correction and with HEAT-Lim [66].

The reader is directed to Kong & Huber (2025; hereafter KH25) for a full discussion of bias-correction methods [65], but in brief, the process was as follows:

1. For every climate model, for each variable of interest (T, p, and q), select data in each climate model's historical output between 1980–2010, as well as during each 20-year GWL period fully contained in the SSP output. The data must be at a 3-hourly temporal interval to capture diurnal temperature patterns.
2. Compute the multi-year average value of each variable at each 3-hourly time-of-day (i.e., January 1st, 00:00 through December 31st, 21:00), averaging across all years within the 1980–2010 period or within each 20-year warming level period. This is an average across years at a fixed clock time, not a resampling of the underlying data: CMIP6 output is used at its native, instantaneous 3-hourly sampling frequency for all but one model, which instead provides 3-hour averages (Supplementary Table S2).
3. For each variable and GWL across all climate models, subtract the value of the 1980–2010 variable from that of the GWL period, constructing 3-hourly resolved "deltas" for each variable.
4. Perform a bilinear interpolation of each climate model-derived delta product such that the grid matches that of the ERA5 output ($0.25° \times 0.25°$).
5. Apply the interpolated delta product for each timestep of the year to all instances of that timestep in the ERA5 reanalysis occurring between 1980–2010. Repeat for each variable and climate model.

"Delta products" derived from all eligible CMIP6 models, both SSP2-4.5 and 5-8.5, and all GWLs of interest are applied to 31 years of ERA5 reanalysis. The effects of climate model biases in mean climate and variability are reduced by applying different model-derived delta products to the historical observation-derived ERA5 reanalysis, thereby enabling more robust projections.

This process deviates from KH25 in two main ways. KH25 defines GWL periods by including all years falling within a 0.5°C interval centered around the warming target. Instead, we define our GWLs using 20-year intervals following Seneviratne & Hauser (2020) [63], which are centered on the first year a warming target is reached and

include the ten years prior and the nine years after. This ensures a consistent length of warming level period among models. Additionally, we choose a different baseline period against which to bias-correct CMIP6 projections. KH25 chose a period of 1950–1976. While this baseline is closer to preindustrial conditions and may contain less of an anthropogenic warming signal, the accuracy of ERA5 data increases substantially upon the introduction of weather satellites in 1979, informing our decision to begin our baseline period after 1979 [67]. Additionally, our longer baseline period may capture more interannual variability.

M_{max} for each of the four considered profiles is calculated using 31 years of bias-corrected T, p, and q for all combinations of climate models, SSPs, and GWLs. These 31 years are then concatenated into a single, continuous M_{max} time series per grid cell, from which summary statistics for each analysis (e.g., warm-season averages, threshold-exceedance counts) are calculated. M_{max} is not calculated over ocean grid cells or Antarctica.

4.5 Demographic datasets

4.5.1 Selecting populous cities

In Figures 1, 2, and S1-S14, decreases in warm season M_{max} and time spent under key M_{max} thresholds are given for twelve highly populated cities. To select these cities, we used the Simplemaps World Cities Database and chose the highest-populated cities with a population of at least 15 million within 5° latitude bands – i.e., although both fall between 20° and 25° N, Guangzhou is chosen and Dhaka is not because the former has a larger population, even though both meet the >15 million population criteria [68].

4.5.2 Demographic projections

Future population heat stress risk is affected by both climate change and population age structure. The ages of populations, in many places, are expected to increase on average due to advances in health care, declining birth rates, and other socioeconomic factors [16–19]. Thus, changes in population demographics must be accounted for when quantifying future heat stress.

To create projections of population heat stress risk, we integrate demographic projections from four sources. Firstly, for future population spatial distribution, we use data from Wang et al, (2022; hereafter W22), which provides 1-km gridded population projections following the SSPs [69]. The SSP2 and SSP5 datasets are coarsened to the same grid as the bias-corrected CMIP6 output ($0.25° \times 0.25°$). However, this dataset does not provide demographic projections of age. Thus, we additionally use the Wittgenstein Center (WIC) Population and Human Capital Projections, which provide age population ratio projections at the country level [45]. These ratios are then fitted to the same grid. The W22 projections can then be scaled by the WIC-derived ratios of the population that fit each of the four HEAT-Lim configurations (children aged 10-19, adults aged 20-64, old adults aged 65-84, and very old adults aged 85+).

For historical population heat stress during the 1980-2010 ERA5 baseline period, we use WorldPop Population Counts [70] and WorldPop Age and Sex Structures [71],

which are then similarly coarsened from a 1-km resolution to a 0.25° × 0.25° grid. Using WorldPop for this baseline period is methodologically consistent with our future population distribution data, as W22's spatial projection model is itself trained on WorldPop grids [69]. We use historical population estimates from the year 2000 to represent our baseline period, as that is as far back as these projections go [70, 71].

W22 population density projections and WIC ratio projections are available from 2020 to 2100 at five-year intervals. To select the appropriate year for each model, GWL, and scenario, each climate model's own year of GWL crossing (Methods 4.3) is rounded to the nearest multiple of five, and the resulting W22/WIC snapshot is paired with that model's own M_{max} output. For example, under SSP5-8.5, ACCESS-CM2 reaches 2°C of global average warming in 2040 and so uses 2040 W22/WIC data, while MIROC6 reaches 2°C later (2055) under the same scenario and uses 2055 data instead. Person-hours are calculated per model using its own matched population year, then averaged across models for a given GWL and scenario.

Unlike Figures 1-3, which are indexed purely to GWL and are therefore not particularly sensitive to which emissions scenario is used to reach a given GWL, Figure 4 also depends on calendar year through this population-year matching, and slower-warming scenarios reach a given GWL later in time. Because global population continues to grow and age throughout the century regardless of emissions pathway, the more moderate SSP2-4.5 scenario pairs each GWL with a larger, older population than SSP5-8.5 does. Consequently, demographic drivers (aging and population density) contribute proportionally more to future PH/yr increases under SSP2-4.5 than under SSP5-8.5 at the same GWL (e.g., at 2°C GWL for the $M_{max} < 4.8$ METs threshold, demographic drivers account for 65.3% of the combined demographic-plus-climate effect under SSP2-4.5, compared to 59.8% under SSP5-8.5).

4.6 Population heat risk calculations

For each age group, we estimate population risk to heat in units of "person-hours" (P) by multiplying the number of hours per year that a given activity level is possible for an age group (hot-hours, H) by the number of people in a given grid cell (density, D) by the proportion of people in that grid cell who fall into that age group (ratio, R). For example, we calculate person-hours of heat risk in a grid cell for adults between the ages of 20–64 as follows:

$$P_{adult} = H_{adult} \times D \times R_{adult} \tag{1}$$

Person-hours are calculated for every age group for the ERA5 baseline period, and for every GWL across climate models. For a given GWL, total person-hours in a grid cell can be calculated by summing the person-hours of all four age groups:

$$P_{total} = P_{kids} + P_{adult} + P_{old} + P_{very\ old} \tag{2}$$

Population heat risk is affected by three drivers in our projections: climate change, population growth, and aging. We can isolate the impacts of a given driver by allowing only a single driver to evolve at a time. For instance, to isolate the impacts of climate change at a given GWL, P_{total} is calculated using the hot-hours of the future GWL (2°C in Figure 4), but the demographic variables (population density and age

proportions) are from the baseline ERA5 period (GWL of 0.7°C). The heat risk at present-day GWLs is subtracted as a baseline to reveal the effect of climate change, e.g.:

$$P_{total,\ climate\ change\ only} = H_{2^\circ\mathrm{C}} \times D_{0.7^\circ\mathrm{C}} \times R_{0.7^\circ\mathrm{C}} - H_{0.7^\circ\mathrm{C}} \times D_{0.7^\circ\mathrm{C}} \times R_{0.7^\circ\mathrm{C}} \quad (3)$$

This process is repeated for the other two drivers to calculate $P_{total,\ density\ change\ only}$ and $P_{total,\ aging\ only}$. To understand which processes most drive person-hour increases in population heat risk, the ratio of $P_{total,\ climate\ change\ only} : P_{total,\ density\ change\ only} : P_{total,\ aging\ only}$ is taken for each country (Figure 4b and 4d). Finer spatial resolution of these calculations is impossible, given that age group ratio information, R, only varies in time on a country-level resolution. Because the underlying demographic datasets do not share identical spatial coverage, only grid cells with valid data in all three individual driver terms are used per country; countries for which this shared-coverage domain represents less than 50% of the country's population are left unshaded in Figure 4b and 4d, since their driver classification would otherwise be based on an unrepresentative subset of the population (21 countries in total, predominantly small island nations and other small or narrow-geometry states – e.g., the Bahamas, Fiji, Vanuatu, Greenland – where a 0.25° grid leaves little margin against country boundaries; full list in Supplementary Table S4). One additional country, Iceland, is left unshaded in Figure 4b for an unrelated reason: it has zero hot-hours under the $M_{max} < 3.3$ METs threshold in the multi-model mean at both the historical baseline and the 2°C GWL, leaving no driver signal to decompose (Supplementary Information, S5).

To calculate the effects of nonlinear interactions between drivers, the cross-term C (Figure 4a and 4c, gray bars) is calculated by subtracting the sum of these three individual driver terms from the future person-hours total where all three drivers are allowed to evolve in time, again with the signal from baseline person-hours subtracted.

$$C = (P_{total,\ 2^\circ\mathrm{C}} - P_{total,\ 0.7^\circ\mathrm{C}}) - (P_{total,\ climate\ change\ only} + P_{total,\ density\ change\ only} + P_{total,\ aging\ only}) \quad (4)$$

To provide context for the person-hours totals reported in the main text, we also calculate the theoretical maximum possible person-hours per year, P_{max}: the total population aged 10 and older (the age range covered by our four physiological profiles; Methods 4.1) summed across all land grid cells, multiplied by the number of hours in a year (8,760). Population under age 10 is excluded from P_{max}, consistent with their exclusion from every P term above.

$$P_{max} = \left(\sum_{\text{grid cells}} D \times (R_{kids} + R_{adult} + R_{old} + R_{very\ old}) \right) \times 8760 \quad (5)$$

P_{max} represents the person-hours that would occur if every person aged 10 or older experienced uncompensable conditions for the entire year. Because global population changes over the century, P_{max} is evaluated using the same GWL-matched population

year as the corresponding P_{total} figure it contextualizes, rather than a single fixed value. At the ERA5 baseline (year 2000), $P_{max} \approx 42.4$ trillion PH/yr; by a 2°C GWL, P_{max} increases to ≈ 58.0 trillion PH/yr under SSP5-8.5 (average year 2042) and ≈ 62.2 trillion PH/yr under SSP2-4.5 (average year 2055), reflecting continued population growth.

Declarations

Funding. H.S. was supported by the U.S. Department of Education's Graduate Assistance in Areas of National Need (GAANN) program (Award No. P200A240042) and by National Science Foundation (NSF) Award No. 2228216. J.K.V. and G.G.-E. were supported by the National Science Foundation (NSF) CAREER Award No. CMMI-2045663. O.J. was supported by a National Health and Medical Research Council (NHMRC) Investigator Grant (No. 2021/GNT2009507). S.E.P.-K. was supported by Australian Research Council (ARC) Grant No. CE230100012. J.W.B. was supported by NOAA's Climate Program Office's Modeling, Analysis, Predictions, and Projections Program, through funds from the Inflation Reduction Act Forward Looking Projections initiative (Grant #NA23OAR4310599).

Competing interests. The authors declare no competing interests.

Data availability. CMIP6 climate model output used in this study is publicly available via the Earth System Grid Federation (ESGF) [59]. ERA5 reanalysis data are publicly available via the Copernicus Climate Data Store [60]. Future population projections are available from Wang et al. (2022) [69] and the Wittgenstein Centre for Demography and Global Human Capital [45]; historical population data are available from WorldPop [70, 71]. HadCRUT5 observational temperature data used to calculate global warming levels are available from the UK Met Office [64]. The derived and processed datasets generated in this study (e.g., gridded M_{max} output and person-hours estimates underlying the figures and tables) are available via Figshare [DOI TBD].

Code availability. The HEAT-Lim model code is available in a Zenodo repository [47]. The code used to apply HEAT-Lim to climate model projections in this study is available on GitHub [48].

Author contributions. H.S. and J.W.B. conceptualized the study. H.S., J.K.V., G.G.-E., O.J., and Q.K. developed the methodology. H.S. and Y.H. performed the formal analysis and investigation and curated the data. H.S. created the visualizations and wrote the original draft. J.W.B. supervised the project. All authors contributed to reviewing and editing the manuscript.

Acknowledgements. H.S. would like to acknowledge Luke Parsons and Kendra Rentz for advancing the HEAT-Lim literature and meaningful scientific conversations, as well as Lilith Duncan for assistance writing code. This work was primarily completed on the traditional, ancestral, and unceded territory of the Acjachemen and Tongva peoples.

References

[1] IPCC: Climate Change 2021: The Physical Science Basis. Contribution of Working Group I to the Sixth Assessment Report of the Intergovernmental Panel on Climate Change, p. 2391. Cambridge University Press, Cambridge, UK and New York, NY, USA (2021). https://doi.org/10.1017/9781009157896 . https://report.ipcc.ch/ar6/wg1/IPCC_AR6_WGI_FullReport.pdf

[2] Perkins-Kirkpatrick, S.E., Lewis, S.C.: Increasing trends in regional heatwaves. Nature Communications **11**(1), 3357 (2020) https://doi.org/10.1038/s41467-020-16970-7

[3] Wang, X.-S., He, L., Ma, X.-H., Bie, Q., Luo, L., Xiong, Y.-C., Ye, J.-S.: The emergence of prolonged deadly humid heatwaves. International Journal of Climatology **42**(16), 8607–8618 (2022) https://doi.org/10.1002/joc.7750 https://rmets.onlinelibrary.wiley.com/doi/pdf/10.1002/joc.7750

[4] Emerton, R., Nicolas, J., Lombardi, A., Di Napoli, C.: Global heat stress intensification and its expanding footprint on the human population. Nature Climate Change (2026) https://doi.org/10.1038/s41558-026-02670-5

[5] Cruz, M., Mach, K.J., Turek-Hankins, L.L., Ashad-Bishop, K.C., Bailey, Z.D., Evans, S.D., Fanning, A., Fernandez-Burgos, M., Gilbert, J., Howard, B., Mahabir, M., Marturano, J., Murphy, L.N., Muse, N., Pérodin, J., Clement, A.C.: Where heat does not come in waves: a framework for understanding and managing chronic heat. Environmental Research: Climate **4**(2), 023002 (2025) https://doi.org/10.1088/2752-5295/adc827

[6] Romanello, M., Walawender, M., Hsu, S.-C., Moskeland, A., Palmeiro-Silva, Y., Scamman, D., Smallcombe, J.W., Abdullah, S., Ades, M., Al-Maruf, A., Ameli, N., Angelova, D., Ayeb-Karlsson, S., Ballester, J., Basagaña, X., Bechara, H., Beggs, P.J., Cai, W., Campbell-Lendrum, D., Charnley, G.E.C., Courtenay, O., Cross, T.J., Dalin, C., Dasandi, N., Dasgupta, S., Davies, M., Eckelman, M., Freyberg, C., Corral, P.G., Gasparyan, O., Giguere, J., Gordon-Strachan, G., Gumy, S., Gunther, S.H., Hamilton, I., Hang, Y., Hänninen, R., Hartinger, S., He, K., Heidecke, J., Hess, J.J., Jankin, S., Jay, O., Pantera, D.K., Kelman, I., Kennard, H., Kiesewetter, G., Kinney: The 2025 report of the lancet countdown on health and climate change: climate change action offers a lifeline. The Lancet **406**(10521), 2804–2857 (2025) https://doi.org/10.1016/s0140-6736(25)01919-1

[7] Vicedo-Cabrera, A.M., Scovronick, N., Sera, F., Royé, D., Schneider, R., Tobias, A., Astrom, C., Guo, Y., Honda, Y., Hondula, D.M., Abrutzky, R., Tong, S., Coelho, M.d.S.Z.S., Saldiva, P.H.N., Lavigne, E., Correa, P.M., Ortega, N.V., Kan, H., Osorio, S., Kyselý, J., Urban, A., Orru, H., Indermitte, E., Jaakkola, J.J.K., Ryti, N., Pascal, M., Schneider, A., Katsouyanni, K., Samoli, E., Mayvaneh, F., Entezari, A., Goodman, P., Zeka, A., Michelozzi, P., de'Donato, F., Hashizume, M., Alahmad, B., Diaz, M.H., Valencia, C.D.L.C., Overcenco, A.,

Houthuijs, D., Ameling, C., Rao, S., Di Ruscio, F., Carrasco-Escobar, G., Seposo, X., Silva, S., Madureira, J., Holobaca, I.H., Fratianni, S., Acquaotta, F., Kim, H., Lee, W., In: The burden of heat-related mortality attributable to recent human-induced climate change. Nature Climate Change **11**(6), 492–500 (2021) https://doi.org/10.1038/s41558-021-01058-x

[8] Chen, K., Schrijver, E., Sivaraj, S., Sera, F., Scovronick, N., Jiang, L., Roye, D., Lavigne, E., Kyselý, J., Urban, A., Schneider, A., Huber, V., Madureira, J., Mistry, M.N., Cvijanovic, I., Armstrong, B., Schneider, R., Tobias, A., Astrom, C., Guo, Y., Honda, Y., Abrutzky, R., Tong, S., Sousa Zanotti Stagliorio Coelho, M., Saldiva, P.H.N., Correa, P.M., Ortega, N.V., Kan, H., Osorio, S., Orru, H., Indermitte, E., Jaakkola, J.J.K., Ryti, N., Pascal, M., Katsouyanni, K., Analitis, A., Mayvaneh, F., Entezari, A., Goodman, P., Zeka, A., Michelozzi, P., de'Donato, F., Hashizume, M., Alahmad, B., Diaz, M.H., Cruz Valencia: Impact of population aging on future temperature-related mortality at different global warming levels. Nature Communications **15**(1) (2024) https://doi.org/10.1038/s41467-024-45901-z

[9] Weinberger, K.R., Haykin, L., Eliot, M.N., Schwartz, J.D., Gasparrini, A., Wellenius, G.A.: Projected temperature-related deaths in ten large u.s. metropolitan areas under different climate change scenarios. Environment International **107**, 196–204 (2017) https://doi.org/10.1016/j.envint.2017.07.006

[10] Gasparrini, A., Guo, Y., Sera, F., Vicedo-Cabrera, A.M., Huber, V., Tong, S., de Sousa Zanotti Stagliorio Coelho, M., Nascimento Saldiva, P.H., Lavigne, E., Matus Correa, P., Valdes Ortega, N., Kan, H., Osorio, S., Kyselý, J., Urban, A., Jaakkola, J.J.K., Ryti, N.R.I., Pascal, M., Goodman, P.G., Zeka, A., Michelozzi, P., Scortichini, M., Hashizume, M., Honda, Y., Hurtado-Diaz, M., Cesar Cruz, J., Seposo, X., Kim, H., Tobias, A., Iñiguez, C., Forsberg, B., Åström, D.O., Ragettli, M.S., Guo, Y.L., Wu, C.-f., Zanobetti, A., Schwartz, J., Bell, M.L., Dang, T.N., Van, D.D., Heaviside, C., Vardoulakis, S., Hajat, S., Haines, A., Armstrong, B.: Projections of temperature-related excess mortality under climate change scenarios. The Lancet Planetary Health **1**(9), 360–367 (2017) https://doi.org/10.1016/S2542-5196(17)30156-0

[11] Sherwood, S.C., Huber, M.: An adaptability limit to climate change due to heat stress. Proceedings of the National Academy of Sciences **107**(21), 9552–9555 (2010) https://doi.org/10.1073/pnas.0913352107 https://www.pnas.org/doi/pdf/10.1073/pnas.0913352107

[12] Vecellio, D.J., Kong, Q., Kenney, W.L., Huber, M.: Greatly enhanced risk to humans as a consequence of empirically determined lower moist heat stress tolerance. Proceedings of the National Academy of Sciences **120**(42), 2305427120 (2023) https://doi.org/10.1073/pnas.2305427120 https://www.pnas.org/doi/pdf/10.1073/pnas.2305427120

[13] Davies-Jones, R.: An efficient and accurate method for computing the wet-bulb temperature along pseudoadiabats. Monthly Weather Review **136**(7), 2764–2785 (2008) https://doi.org/10.1175/2007mwr2224.1

[14] Lu, Y.-C., Romps, D.M.: Predicting fatal heat and humidity using the heat index model. Journal of Applied Physiology **134**(3), 649–656 (2023) https://doi.org/10.1152/japplphysiol.00417.2022 https://doi.org/10.1152/japplphysiol.00417.2022. PMID: 36701484

[15] Vargas Zeppetello, L.R., Raftery, A.E., Battisti, D.S.: Probabilistic projections of increased heat stress driven by climate change. Communications Earth & Environment **3**(1) (2022) https://doi.org/10.1038/s43247-022-00524-4

[16] Naja, S., Din Makhlouf, M.M.E., Chehab, M.A.H.: An ageing world of the 21st century: a literature review. International Journal Of Community Medicine And Public Health **4**(12), 4363–4369 (2017) https://doi.org/10.18203/2394-6040.ijcmph20175306

[17] Lunenfeld, B., Stratton, P.: The clinical consequences of an ageing world and preventive strategies. Best Practice & Research Clinical Obstetrics & Gynaecology **27**(5), 643–659 (2013) https://doi.org/10.1016/j.bpobgyn.2013.02.005 . Science of healthy Aging in Women

[18] Cheng, H., Luo, W., Si, S., Xin, X., Peng, Z., Zhou, H., Liu, H., Yu, Y.: Global trends in total fertility rate and its relation to national wealth, life expectancy and female education. BMC Public Health **22**(1) (2022) https://doi.org/10.1186/s12889-022-13656-1

[19] pp. 22–28. United Nations (2023). https://doi.org/10.18356/9789210052467c007 . http://dx.doi.org/10.18356/9789210052467c007

[20] Falchetta, G., De Cian, E., Sue Wing, I., Carr, D.: Global projections of heat exposure of older adults. Nature Communications **15**(1) (2024) https://doi.org/10.1038/s41467-024-47197-5

[21] Pal, J.S., Eltahir, E.A.B.: Future temperature in southwest asia projected to exceed a threshold for human adaptability. Nature Climate Change **6**(2), 197–200 (2015) https://doi.org/10.1038/nclimate2833

[22] Coffel, E.D., Horton, R.M., Sherbinin, A.: Temperature and humidity based projections of a rapid rise in global heat stress exposure during the 21st century. Environmental Research Letters **13**(1), 014001 (2017) https://doi.org/10.1088/1748-9326/aaa00e

[23] Im, E.-S., Pal, J.S., Eltahir, E.A.B.: Deadly heat waves projected in the densely populated agricultural regions of south asia. Science Advances **3**(8), 1603322 (2017) https://doi.org/10.1126/sciadv.1603322

https://www.science.org/doi/pdf/10.1126/sciadv.1603322

[24] Safieddine, S., Clerbaux, C., Clarisse, L., Whitburn, S., Eltahir, E.A.B.: Present and future land surface and wet bulb temperatures in the arabian peninsula. Environmental Research Letters **17**(4), 044029 (2022) https://doi.org/10.1088/1748-9326/ac507c

[25] Vanos, J.K., Baldwin, J.W., Jay, O., Ebi, K.L.: Simplicity lacks robustness when projecting heat-health outcomes in a changing climate. Nature Communications **11**(1) (2020) https://doi.org/10.1038/s41467-020-19994-1

[26] Vanos, J., Guzman-Echavarria, G., Baldwin, J.W., Bongers, C., Ebi, K.L., Jay, O.: A physiological approach for assessing human survivability and liveability to heat in a changing climate. Nature Communications **14**(1) (2023) https://doi.org/10.1038/s41467-023-43121-5

[27] Kenney, W.L., Cottle, R.M., Vecellio, D.J., Fisher, K.G., Leach, O.K., Kong, Q., Wolf, S.T.: Age and livability in a hotter climate. eBioMedicine **122**, 106020 (2025) https://doi.org/10.1016/j.ebiom.2025.106020

[28] Parsons, L.A., Baldwin, J.W., Guzman-Echavarria, G., Jay, O., Kalmus, P., Staudmyer, H., Vanos, J.K., Wolff, N.H.: Intensifying global heat threatens livability for younger and older adults. Environmental Research: Health **4**(1), 015013 (2026) https://doi.org/10.1088/2752-5309/ae3c3a

[29] Xu, X., Rioux, T.P., Castellani, J.W., Montain, S.J., Charkoudian, N.: Validation of livability environmental limits to heat and humidity. Journal of Applied Physiology **137**(6), 1642–1648 (2024) https://doi.org/10.1152/japplphysiol.00225.2024 https://doi.org/10.1152/japplphysiol.00225.2024. PMID: 39540826

[30] Perkins-Kirkpatrick, S.E., Gregory, C.H., Vanos, J.K., Baldwin, J.W., Staudmyer, H., Guzman-Echavarria, G., Jay, O.: Deadly heat stress conditions are already occurring. Nature Communications **17**(1) (2026) https://doi.org/10.1038/s41467-026-70485-1

[31] Morrison, S.F., Nakamura, K.: Central mechanisms for thermoregulation. Annual Review of Physiology **81**(1), 285–308 (2019) https://doi.org/10.1146/annurev-physiol-020518-114546

[32] Cramer, M.N., Jay, O.: Partitional calorimetry. Journal of Applied Physiology **126**(2), 267–277 (2019) https://doi.org/10.1152/japplphysiol.00191.2018 https://doi.org/10.1152/japplphysiol.00191.2018. PMID: 30496710

[33] Dunne, J.P., Stouffer, R.J., John, J.G.: Reductions in labour capacity from heat stress under climate warming. Nature Climate Change **3**(6), 563–566 (2013) https://doi.org/10.1038/nclimate1827

[34] Parsons, L.A., Shindell, D., Tigchelaar, M., Zhang, Y., Spector, J.T.: Increased labor losses and decreased adaptation potential in a warmer world. Nature Communications **12**(1) (2021) https://doi.org/10.1038/s41467-021-27328-y

[35] Baldwin, J.W., Benmarhnia, T., Ebi, K.L., Jay, O., Lutsko, N.J., Vanos, J.K.: Humidity's role in heat-related health outcomes: A heated debate. Environmental Health Perspectives **131**(5) (2023) https://doi.org/10.1289/ehp11807

[36] Baldwin, J.W., Dessy, J.B., Vecchi, G.A., Oppenheimer, M.: Temporally compound heat wave events and global warming: An emerging hazard. Earth's Future **7**(4), 411–427 (2019) https://doi.org/10.1029/2018EF000989

[37] Nelson, G.C., Vanos, J., Havenith, G., Jay, O., Ebi, K.L., Hijmans, R.J.: Global reductions in manual agricultural work capacity due to climate change. Global Change Biology **30**(1), 17142 (2024) https://doi.org/10.1111/gcb.17142

[38] Oh, S.-G., Son, S.-W., Hong, D.-C.: Increasing physical work capacity losses due to heat stress increase. International Journal of Biometeorology **69**(11), 3073–3083 (2025) https://doi.org/10.1007/s00484-025-03008-0

[39] Matthews, T., Raymond, C., Foster, J., Baldwin, J.W., Ivanovich, C., Kong, Q., Kinney, P., Horton, R.M.: Mortality impacts of the most extreme heat events. Nature Reviews Earth & Environment **6**(3), 193–210 (2025) https://doi.org/10.1038/s43017-024-00635-w

[40] Larose, J., Boulay, P., Sigal, R.J., Wright, H.E., Kenny, G.P.: Age-related decrements in heat dissipation during physical activity occur as early as the age of 40. PLoS ONE **8**(12), 83148 (2013) https://doi.org/10.1371/journal.pone.0083148

[41] Fleg, J.L., Morrell, C.H., Bos, A.G., Brant, L.J., Talbot, L.A., Wright, J.G., Lakatta, E.G.: Accelerated longitudinal decline of aerobic capacity in healthy older adults. Circulation **112**(5), 674–682 (2005) https://doi.org/10.1161/CIRCULATIONAHA.105.545459

[42] Woollings, T., Barriopedro, D., Methven, J., Son, S.-W., Martius, O., Harvey, B., Sillmann, J., Lupo, A.R., Seneviratne, S.: Blocking and its response to climate change. Current Climate Change Reports **4**(3), 287–300 (2018) https://doi.org/10.1007/s40641-018-0108-z

[43] Zha, J., Shen, C., Li, Z., Wu, J., Zhao, D., Fan, W., Sun, M., Azorin-Molina, C., Deng, K.: Projected changes in global terrestrial near-surface wind speed in 1.5°c–4.0°c global warming levels. Environmental Research Letters **16**(11), 114016 (2021) https://doi.org/10.1088/1748-9326/ac2fdd

[44] Liu, S., Song, F., Wang, Y., Dong, L., Geng, Y.-F., Zhang, Y.: Polar dimming and mid-latitude brightening in a warming climate. National Science Review **13**(13) (2026) https://doi.org/10.1093/nsr/nwag330

[45] KC, S., Moradhvaj, Potancokova, M., Adhikari, S., Yildiz, D.: Wittgenstein Center (WIC) Population and Human Capital Projections – 2023 (2023). https://doi.org/10.5281/zenodo.14718294 . https://zenodo.org/records/14718294

[46] Jay, O., Vanos, J., Gagnon, D., Tartarini, F.: To save lives in heatwaves, focus on how human bodies work. Nature **644**(8075), 35–38 (2025) https://doi.org/10.1038/d41586-025-02461-6

[47] Guzman-Echavarria, G., Vanos, J.: ASU/USYD HEAT-Lim (Human/Environmental Adaptation and Threshold Limits Model): Physiological-based estimations of human survivability and liveability under extreme heat in a changing climate (2025). https://doi.org/10.5281/zenodo.15642387 . https://zenodo.org/records/15642387

[48] Staudmyer, H.: Code for: Humanity's Future Capacity for Physical Activity Limited by Climate Change and Population Aging (2026). https://github.com/Halmarsta18/Staudmyer_et_al_2026

[49] Falk, B., Dotan, R.: Children's thermoregulation during exercise in the heat – a revisit. Applied Physiology, Nutrition, and Metabolism **33**(2), 420–427 (2008) https://doi.org/10.1139/H07-185

[50] Tsuzuki, K.: Physiological and behavioural responses to heat among children and older adults. Building and Environment (2023)

[51] Inbar, O., Morris, N., Epstein, Y., Gass, G.: Comparison of thermoregulatory responses to exercise in dry heat among prepubertal boys, young adults and older males. Experimental Physiology **89**(6), 691–700 (2004) https://doi.org/10.1113/expphysiol.2004.027979

[52] Morris, N.B., English, T., Hospers, L., Capon, A., Jay, O.: The effects of electric fan use under differing resting heat index conditions: A clinical trial. Annals of Internal Medicine **171**(9), 675–677 (2019) https://doi.org/10.7326/m19-0512

[53] Fisher, K.G., Vecellio, D.J., Cottle, R.M., Leach, O.K., Wolf, S.T., Kenney, W.L.: Lower maximal skin wettedness in both warm-humid and hot-dry environments with advanced age (psu heat project). Journal of Applied Physiology **137**(6), 1549–1553 (2024) https://doi.org/10.1152/japplphysiol.00758.2024

[54] Fisher, K.G., Leach, O.K., Cottle, R.M., Kenney, W.L.: Maximal skin wettedness as a function of environment and metabolic rate in unacclimated young and older adults (psu heat project). International Journal of Biometeorology **69**(10), 2711–2718 (2025) https://doi.org/10.1007/s00484-025-02986-5

[55] European Commission, Joint Research Centre: Expofacts: the european exposure factors sourcebook. Technical report (2013). https://joint-research-centre.ec.europa.eu/expofacts-european-exposure-factorssourcebook_en

[56] Phillips, L.J., Moya, J.: Exposure factors resources: contrasting epa's exposure factors handbook with international sources. Journal of Exposure Science & Environmental Epidemiology **24**(3), 233–243 (2013) https://doi.org/10.1038/jes.2013.17

[57] U.S. Environmental Protection Agency: Exposure factors handbook: 2011 edition. Technical report (2011)

[58] Schreier, S.F., Suomi, I., Bröde, P., Formayer, H., Rieder, H.E., Nadeem, I., Jendritzky, G., Batchvarova, E., Weihs, P.: The uncertainty of utci due to uncertainties in the determination of radiation fluxes derived from numerical weather prediction and regional climate model simulations. International Journal of Biometeorology **57**(2), 207–223 (2013) https://doi.org/10.1007/s00484-012-0525-y

[59] Eyring, V., Bony, S., Meehl, G.A., Senior, C.A., Stevens, B., Stouffer, R.J., Taylor, K.E.: Overview of the coupled model intercomparison project phase 6 (cmip6) experimental design and organization. Geoscientific Model Development **9**(5), 1937–1958 (2016) https://doi.org/10.5194/gmd-9-1937-2016

[60] Hersbach, H., Bell, B., Berrisford, P., Hirahara, S., Horányi, A., Muñoz-Sabater, J., Nicolas, J., Peubey, C., Radu, R., Schepers, D., Simmons, A., Soci, C., Abdalla, S., Abellan, X., Balsamo, G., Bechtold, P., Biavati, G., Bidlot, J., Bonavita, M., De Chiara, G., Dahlgren, P., Dee, D., Diamantakis, M., Dragani, R., Flemming, J., Forbes, R., Fuentes, M., Geer, A., Haimberger, L., Healy, S., Hogan, R.J., Hólm, E., Janisková, M., Keeley, S., Laloyaux, P., Lopez, P., Lupu, C., Radnoti, G., Rosnay, P., Rozum, I., Vamborg, F., Villaume, S., Thépaut, J.-N.: The era5 global reanalysis. Quarterly Journal of the Royal Meteorological Society **146**(730), 1999–2049 (2020) https://doi.org/10.1002/qj.3803

[61] Evin, G., Ribes, A., Corre, L.: Assessing cmip6 uncertainties at global warming levels. Climate Dynamics **62**(8), 8057–8072 (2024) https://doi.org/10.1007/s00382-024-07323-x

[62] Falkner, R.: The paris agreement and the new logic of international climate politics. Technical report, Grantham Research Institute on Climate Change and the Environment, LSE (2016). https://www.lse.ac.uk/granthaminstitute/wp-content/uploads/2016/10/Falkner_2016_TheParisAgreement.pdf

[63] Seneviratne, S.I., Hauser, M.: Regional climate sensitivity of climate extremes in cmip6 versus cmip5 multimodel ensembles. Earth's Future **8**(9), 2019–001474 (2020) https://doi.org/10.1029/2019EF001474

[64] Morice, C.P., Kennedy, J.J., Rayner, N.A., Winn, J.P., Hogan, E., Killick, R.E., Dunn, R.J.H., Osborn, T.J., Jones, P.D., Simpson, I.R.: An updated assessment of near-surface temperature change from 1850: The hadcrut5 data set. Journal of Geophysical Research: Atmospheres **126**(3), 2019–032361 (2020) https://doi.

org/10.1029/2019JD032361

[65] Kong, Q., Huber, M.: A global high-resolution and bias-corrected dataset of cmip6 projected heat stress metrics. Scientific Data **12**(1), 246 (2025) https://doi.org/10.1038/s41597-025-04527-6

[66] May, R.M., Goebbert, K.H., Thielen, J.E., Leeman, J.R., Camron, M.D., Bruick, Z., Bruning, E.C., Manser, R.P., Arms, S.C., Marsh, P.T.: Metpy: A meteorological python library for data analysis and visualization. Bulletin of the American Meteorological Society **103**(10), 2273–2284 (2022) https://doi.org/10.1175/BAMS-D-21-0125.1

[67] Pailleux, J.: The impact of satellite data on global numerical weather prediction (1987) https://doi.org/10.1007/978-94-009-3881-6_9

[68] Simplemaps World Cities Database. https://simplemaps.com/data/world-cities

[69] Wang, X., Meng, X., Long, Y.: Projecting 1 km-grid population distributions from 2020 to 2100 globally under shared socioeconomic pathways. Scientific Data **9**(1), 563 (2022) https://doi.org/10.1038/s41597-022-01675-x

[70] WorldPop Population Counts. https://hub.worldpop.org/geodata/listing?id=64

[71] WorldPop Age and Sex Structures. https://hub.worldpop.org/geodata/listing?id=65

[72] Cramer, M.N., Gagnon, D., Laitano, O., Crandall, C.G.: Human temperature regulation under heat stress in health, disease, and injury. Physiological Reviews **102**(4), 1907–1989 (2022) https://doi.org/10.1152/physrev.00047.2021 PMID: 35679471

Supplementary Files

This is a list of supplementary files associated with this preprint. Click to download.

- SUPPLEMENTStaudmyeretalFINAL.pdf